

Testing Climate Models Using Thermal Infrared Spectra

Stephen Leroy* James Anderson John Dykema Richard Goody

Harvard School of Engineering and Applied Science, Harvard University

J. Climate, Revised, September 7, 2007

Abstract

We present an approach to testing climate models with observations. In this approach, it is possible to directly observe the longwave feedbacks of the climate system in timeseries of annual average outgoing longwave spectra. Tropospheric temperature, stratospheric temperature, water vapor, and carbon dioxide have clear and distinctive signatures in the infrared spectrum, and it is possible to detect trends of these signals unambiguously from trends in the outgoing longwave spectrum by optimal detection techniques. We apply this approach to clear-sky data in the Tropics simulated from the output of an ensemble of climate models. Estimates of the water vapor-longwave feedback by this approach agree to within estimated errors with truth, and it is likely that an uncertainty of 50% can be obtained in twenty years of a continuous timeseries. The correlation of tropospheric temperature and water vapor anomalies can provide a constraint on the water vapor-longwave feedback to 5% uncertainty in twenty years, or 7% in ten years. Thus, it should be possible to place a strong constraint on climate models, which currently show a range of 30% in the water vapor-longwave feedback, in just ten years' time. These results may not hold in the presence of clouds, however, and so it may be necessary to supplement timeseries of outgoing longwave spectra with GPS radio occultation data, which is insensitive to clouds.

1. Introduction

Under prescribed forcing scenarios, sophisticated global climate models still vary by approximately a factor of 2 in their projections for future trends in the global atmosphere. In the third assessment report of the Intergovernmental Panel on Climate Change (IPCC), climate models ranged from 2K to 5K in the projections for global average surface air temperature increase in response to a doubling of carbon dioxide (Houghton et al. 2001). Roughly the same range of projections is found in the ensemble of climate models assembled for the IPCC's Fourth Assessment Report (AR4). Even though it has recently been shown that climate models realize different radiative forcing for the same increases in well-mixed greenhouse gases (Collins et al. 2006), nevertheless much of the uncertainty in climate projection arises from the manner in which different climate models respond to the radiative forcing by increasing well-mixed greenhouse gases. If a capability to predict future climates on interdecadal time scales is desired, it will be necessary to test the projections of current climate models using credible data sets (Goody et al. 1998, 2002) and to verify that these projections are made for the cor-

rect physical reasons.

Climate models vary in their projections of future climates because of the disparate ways that model physics are implemented. The physics of a climate model is a term commonly invoked to refer to parameterizations of physical processes that cannot be integrated by the equations of motion because they are unresolved spatially and/or temporally by a climate model. While there might be a most ideal tuning of the parameters of model physics, uncertainty in those parameters implies a wide range of model response to a prescribed radiative forcing scenario. An alternative way of viewing model response to prescribed radiative forcing is through the paradigm of radiative feedbacks: surface warming can lead to trends in other climate variables which might in turn increase or decrease radiative forcing of the troposphere (North et al. 1981). A recent paper offered a review of radiative feedbacks in the atmosphere, particular the uncertainties associated with each (Bony et al. 2006). Even if a climate model accurately predicts trends in global surface air temperature, that model will only gain widespread credibility if it does so through the right combination of radiative feedbacks.

* *Corresponding author address*: Stephen Leroy, Anderson Group, 12 Oxford St., Link Building, Cambridge, MA 02138.
E-mail: leroy@huarp.harvard.edu

Hence, some way of observing not only overall climate sensitivity but also individual radiative feedbacks is necessary.

The recent emergence of climate benchmark data offers the potential to constrain climate models according to their predictive capability. Here we refer to a data set as a climate benchmark if it is repeatable over arbitrarily long time baselines in such a way that derived trends are broadly credible. Technologically, this is done by assuring that the observations are made traceable to international standards (Pollock et al. 2003) and sampling is adequate. In laboratory work it has also been shown that high spectral resolution thermal infrared radiance spectra can be made traceable to international standards (Dykema and Anderson 2006), and it has also been shown that high spectral resolution outgoing longwave radiation is a potential climate benchmark when satellite-borne (Anderson et al. 2004; Kirk-Davidoff et al. 2005). The NOAA/NASA Decadal Survey of the U.S. National Research Council has called for the deployment of such an instrument (National Research Council, Committee on Earth Science and Applications from Space 2007). It has yet to be shown how trends in the outgoing longwave spectrum might be used to test the projections of climate models.

The outgoing longwave spectrum (OLS) is potentially rich in information content on the radiative balance of the climate system. By virtue of outgoing longwave radiation's role in the energy balance of the climate system, it should also be possible to use outgoing longwave spectra to observe the climate's response to radiative forcing and the feedbacks involved. Kiehl (1983) suggested using the ν_2 rotational band of CO_2 in the infrared to prove greenhouse forcing of the climate. Charlock (1984) supported this point with more sophisticated simulations of emitted radiance spectra and showed that trends in carbon dioxide and temperature would have distinctive spectral signatures over long time periods if observed with sufficiently high spectral resolution. Slingo and Webb (1997) augmented these points with a simulation of a trend in specific humidity and suggested that the water vapor-longwave feedback might be discernible in trends in the emitted infrared spectrum. They left the question of how one might discern the water vapor-longwave feedback using trend data an open one. Harries et al. (2001) have shown that the difference between two thermal infrared data sets obtained 27 years apart reveals the increased radiative forcing by individual greenhouse gases. In this paper, we show how one can discern radiative forcing by carbon dioxide and longwave feedbacks in trends of the emitted infrared spectrum. We perform a study similar to that of Leroy et al. (2006) to discover how outgoing

longwave spectra can be used to test climate models. As in Leroy et al. (2006), we use optimal detection methods (Hasselmann 1993, 1997; North et al. 1995), but here we seek to simultaneously detect multiple climate signals—rather than just a single climate signal—and establish the probability that observed trends are not the results of natural variations of the climate.

The ensemble of runs of climate models by the Intergovernmental Panel for Climate Change's Fourth Assessment Report, now the World Climate Research Programme's (WCRP's) Coupled Model Intercomparison Project phase 3 (CMIP3) multi-model dataset, offers an opportunity to test the methodology we propose by simulating artificial data sets. Because the CMIP3 archive provides model output of three-dimensional pressure, temperature and humidity fields but little on cloud properties, it is only possible to simulate clear sky radiance; hence, we cannot at this point investigate how outgoing longwave spectra might constrain the cloud-longwave feedback. Nevertheless, we are still able to investigate how outgoing longwave spectra might be used to constrain the water vapor-longwave feedback. Because the outgoing longwave spectrum is so strongly influenced by clouds, our conclusions concerning detectibility of the water vapor-longwave feedback come with the strong caveat that a final analysis must in some way account for the influence of clouds on longwave spectra. Bony et al. (2006) show that the climate models in the CMIP3 archive have water vapor-longwave feedbacks that range from 1.5 to 2.2 $\text{W m}^{-2} \text{K}^{-1}$. A useful test of these climate models should provide a more precise observation of the water vapor-longwave feedback than spanned by the CMIP3 models.

In the second section of this paper we discuss the formulation of the problem of detecting climate signals in outgoing longwave spectra. We account for signal shape uncertainty in optimal detection (Huntingford et al. 2006). In the third section we present the results of our exercise in optimal detection using simulated outgoing longwave spectra. In the fourth section we discuss the implications for testing climate models. In the fifth and final section we present a summary and conclusions.

2. Formulation of the problem

We adopt the view of climate feedbacks presented in Wetherald and Manabe (1988) which has also been adopted elsewhere (Held and Soden 2000; Colman 2003; Bony et al. 2006; Soden and Held 2006). In this view, surface temperature plays the dominant role in cooling the Earth system. Fluctuations in this longwave cooling are directly proportional to surface temperature fluctuations ΔT , and are thus written $\Gamma \Delta T$. Other meteorological variables and atmospheric constituents act

to either enhance or suppress the radiation emitted from the Earth system, again proportionally to ΔT . These are the atmospheric feedbacks, and they are defined as

$$\gamma_i^{\text{LW}} \equiv \frac{\partial F^{\text{LW}}}{\partial x_i} \frac{dx_i}{dT} \quad (1)$$

$$\gamma_i^{\text{SW}} \equiv \frac{\partial F^{\text{SW}}}{\partial x_i} \frac{dx_i}{dT} \quad (2)$$

$$\Gamma \equiv -\frac{\partial F^{\text{LW}}}{\partial T} \quad (3)$$

with F^{LW} and F^{SW} being the downward longwave and shortwave fluxes at the tropopause and x_i the value of any group of meteorological variables or the concentration of any atmospheric constituent that then gives its name to the feedback. If a radiative perturbation is applied to the climate by an anthropogenic constituent, then the climate re-achieves radiative balance by changing surface temperature such that the radiative forcing ΔF_{rad} is balanced by a net change in shortwave and longwave radiation at the tropopause:

$$\Delta F_{\text{rad}} + \sum_i \gamma_i^{\text{LW}} \Delta T + \sum_i \gamma_i^{\text{SW}} \Delta T = \Gamma \Delta T, \quad (4)$$

the solution for the response ΔT being

$$\Delta T = \Delta F_{\text{rad}} \left[\Gamma - \sum_i \gamma_i^{\text{LW}} - \sum_i \gamma_i^{\text{SW}} \right]^{-1}. \quad (5)$$

The longwave and shortwave feedback gain terms (γ_i^{LW} and γ_i^{SW}) act to suppress the net surface temperature response when negative and act to enhance the response when positive.

In the longwave, the individual feedback gain terms have corresponding spectral signatures because the change in radiative flux due to a change in a single meteorological variable or atmospheric constituent ($\partial F_{\nu}^{\text{LW}} / \partial x_i$) is distinctive. The gain terms and surface blackbody term are decomposed spectrally $\gamma_{\nu,i}^{\text{LW}}$ as

$$\gamma_{\nu,i}^{\text{LW}} = \frac{\partial F_{\nu}^{\text{LW}}}{\partial x_i} \frac{dx_i}{dT} \quad (6)$$

$$\Gamma_{\nu} = -\frac{\partial F_{\nu}^{\text{LW}}}{\partial T}. \quad (7)$$

The integrals over frequency ν of the spectrally decomposed feedback gains give the feedback gains γ_i . Because the individual $\gamma_{\nu,i}^{\text{LW}}$ have distinct spectral structure, it should be possible to identify how much each feedback has contributed to trends in the emitted longwave spectrum. Optimal detection is ideally suited to this task because it is intended to distinguish between different signals according to the distinctive features of their patterns and because it seeks out those components

of the signal which are associated with relatively little natural interannual variability.

First we describe how we form spectral infrared signatures and then we describe how we apply optimal detection with an accounting for signal shape uncertainty to trends in the outgoing longwave spectrum.

a. Spectral infrared signals

Bony et al. (2006) present three methods of diagnosing feedbacks in a climate model. We use the approach to which they refer as the partial radiative perturbation approach (PRP), as do Held and Soden (2000) and Soden and Held (2006), in their survey of the water vapor feedback in the CMIP3 models. In the PRP approach, the radiative impact of water vapor is determined by comparing the outgoing longwave radiation, as determined by the model's radiative transfer algorithm run off-line, from the evolving temperature and humidity fields to the outgoing longwave radiation from the evolving temperature field but with humidity fixed at its initial values. These radiation calculations are performed *after* the climate model, with temperature and humidity fields varying according to the usual prognostic equations, has been run.

Instead of using a model's radiative transfer module to compute the radiative influence of water vapor, we instead use MODTRAN version 4 (Berk et al. 1998) run in its clear-sky mode at 1 cm^{-1} resolution to obtain the spectral signature of the outgoing longwave radiation. Additionally, instead of subtracting outgoing radiation of the first ten years of a model run from the last ten years, we use linear regression over a long time-series of outgoing longwave spectra. In particular, if we take humidity as q , temperature as T , each dependent on a longitude-latitude coordinate \mathbf{r} , pressure p , month of year m and year t , we find the best linear fit for T and q over the first 50 years of model output of a forced run by

$$T(\mathbf{r}, p, m, t) = T_0(\mathbf{r}, p, m) \quad (8)$$

$$+ t \frac{dT}{dt}(\mathbf{r}, p, m) + dT(\mathbf{r}, p, m, t)$$

$$\ln q(\mathbf{r}, p, m, t) = \ln q_0(\mathbf{r}, p, m) \quad (9)$$

$$+ t \frac{d \ln q}{dt}(\mathbf{r}, p, m) + d \ln q(\mathbf{r}, p, m, t)$$

where slopes dT/dt , $d \ln q/dt$ and intercepts T_0 , q_0 are determined by ordinary linear regression and dT and $d \ln q$ are the departures of temperature and specific humidity from a straight line due to natural inter-annual variability. In the construction of the spectral signal corresponding to longwave forcing by water vapor, we compute two timeseries of outgoing longwave spectra,

one with both temperature and specific humidity varying ($I_{\nu,1}$), and the other with temperature varying but with specific humidity fixed to its intercept value q_0 ($I_{\nu,2}$). Here we let F_ν represent the forward radiance calculation as performed by MODTRAN:

$$I_{\nu,1}(\mathbf{r}, m, t) = F_\nu(T(\mathbf{r}, p, m, t), q(\mathbf{r}, p, m, t)) \quad (10)$$

$$I_{\nu,2}(\mathbf{r}, m, t) = F_\nu(T(\mathbf{r}, p, m, t), q_0(\mathbf{r}, p, m)). \quad (11)$$

The radiative forcing signature of water vapor is found by subtracting the trend of $I_{\nu,2}$ from the trend of $I_{\nu,1}$, both found by linear regression over the first 50 years of a forced run. The dimensions of the signal, then, are (power) (area)⁻¹ (frequency)⁻¹ (solid angle)⁻¹ (time)⁻¹.

In Fig. 1 we illustrate how spectral infrared signals are constructed. We have computed five radiance spectra trends based on fixing various combinations of carbon dioxide, temperature, stratospheric temperature, and specific humidity at their intercept values by forming appropriate linear combinations. For example, in order to obtain the carbon dioxide signal, we subtract the simulation with carbon dioxide fixed from a like simulation but with carbon dioxide increasing. Likewise, in order to obtain the longwave spectral signature of tropospheric temperature, we subtract the simulation with carbon dioxide and tropospheric temperature fixed from the simulation with carbon dioxide fixed but with tropospheric temperature changing according to model output.

We distinguish between tropospheric temperature trends and stratospheric temperature trends because temperature response to increased carbon dioxide in the two regions depends on different physics. The climate feedbacks do not apply as strongly in the stratosphere, where radiative balance is achieved in large part by radiative cooling by carbon dioxide. Also, the pattern of stratospheric cooling simulated by the different CMIP3 models cannot be expected to agree because of their different methods of accounting for ozone. For these reasons we distinguish between trends in outgoing longwave radiance spectra due to tropospheric temperature trends and stratospheric temperature trends. We define the tropical stratosphere as all model levels above (lower pressures than) 100 hPa. For our purposes, the definition of the stratosphere need not be any more rigorous than this; whatever the flaws in the definition of the stratosphere, a proper accounting for signal shape uncertainty (see below) should make up the deficit.

The lower panel of Fig. 1 shows the four signals we choose to detect in outgoing longwave spectral radiance trends: a carbon dioxide signal s_{CO_2} , a tropospheric temperature signal $s_{T_{\text{trop}}}$, a stratospheric temperature signal $s_{T_{\text{strat}}}$, and a water vapor signal $s_{\text{water vapor}}$.

They are related to the feedbacks in Eq. 3 by

$$s_{\text{CO}_2} = -\frac{\partial F_{\nu,\text{rad}}}{\partial [\text{CO}_2]} \frac{d[\text{CO}_2]}{dt} \quad (12)$$

$$s_{T_{\text{trop}}} = (\Gamma_\nu - \gamma_{\nu,\text{lapse rate}}) \times \frac{dT}{dt} \quad (13)$$

$$s_{T_{\text{strat}}} = -\frac{\partial F^{\text{LW}}}{\partial T_{\text{strat}}} \frac{dT_{\text{strat}}}{dt} \quad (14)$$

$$s_{\text{water vapor}} = -\gamma_{\nu,\text{water vapor}} \times \frac{dT}{dt}. \quad (15)$$

All signals are constructed over the Tropics only, defined to lie within 25°S and 25°N. We have used the output of the SRES-A1B radiative forcing scenario to construct the signals and performed linear regressions over the first 50 yrs of output. The carbon dioxide signal is the same as that produced in Charlock (1984) and the other signals are the same as those produced in Slingo and Webb (1997).

b. Optimal detection

Optimal detection techniques allow a determination of the amplitude of one or multiple signals with prescribed shape(s) in a timeseries of data in a way that minimizes the influence of naturally occurring fluctuations of the climate system. Optimal detection is complicated by an ambiguous inversion of a covariance matrix describing natural variability. Allen and Tett (1999) give a criterion for truncation of the matrix inversion that calls for consistency between post-fit residuals and the prescription of natural variability. This approach has been used in most climate signal detection and attribution studies (Hegerl et al. 2000; Stott et al. 2000b,a; Tett et al. 2002; Santer et al. 2003). Application of this approach to detection in the infrared spectrum leads to a truncation of the signal space so severe that optimal detection no longer succeeds in detecting signals on decadal time scales. We instead adopt the approach to optimal detection that includes signal shape uncertainty.

Optimal detection that includes signal shape uncertainty (Huntingford et al. 2006) resolves the ambiguity in inverting the natural variability covariance matrix by considering uncertainties in the prescribed signals' shapes. Components of natural variability that are undersampled are generally associated with fine-scale details of climate signal shapes, and standard optimal detection methods inappropriately skew detection toward those components. In accounting for uncertainty in signals' shapes, those components become irrelevant, thus stabilizing detection. Posterior uncertainty estimates for the presence of a signal in a timeseries of data asymptote to a non-zero value with increasing truncation of the detection space when uncertainty in signal shape is accounted for.

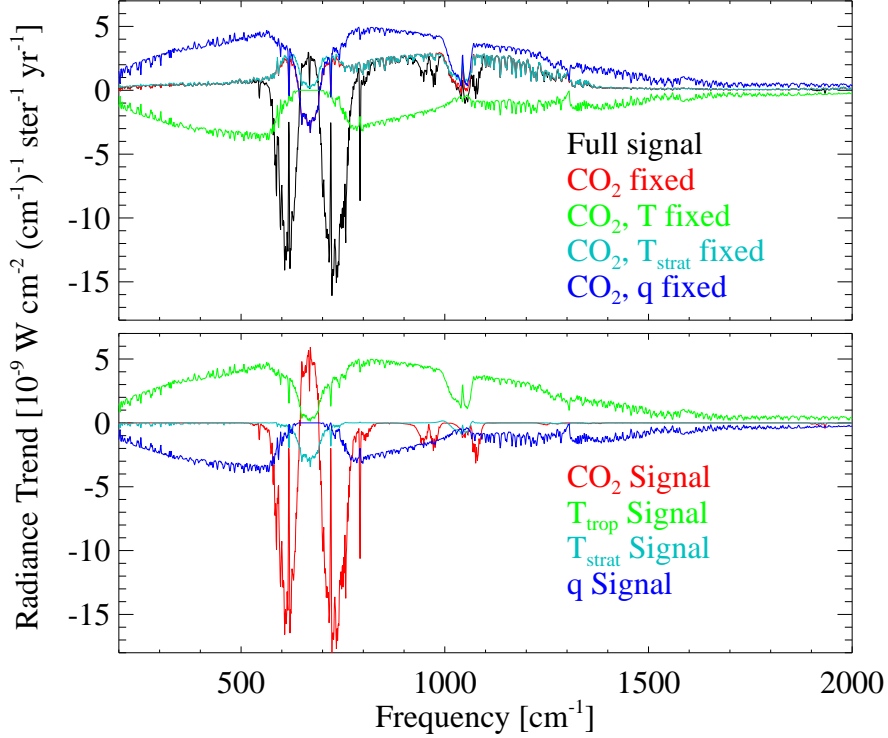


FIG. 1. Construction of spectral infrared signals. The top panel shows spectral radiance trends from five simulations of trends in outgoing longwave radiance spectra: the full signal, carbon dioxide fixed to its intercept value (red), carbon dioxide and temperature fixed to their intercept values (green), carbon dioxide and stratospheric temperature fixed to their intercept values (turquoise), and carbon dioxide and specific humidity fixed to their intercept values (blue). The lower panel shows the deduced radiance signals: the carbon dioxide signal (red), the tropospheric temperature signal (green), the stratospheric temperature signal (turquoise), and the specific humidity signal (blue). The ordinate's units are $W\text{ cm}^{-2}\text{ ster}^{-1}(\text{cm}^{-1})^{-1}\text{ yr}^{-1}$. The first 50 years of the SRES-A1B run of the NCAR CCSM3 climate model were used. Spectra are spatially averaged over the Tropics, 25°S to 25°N .

Briefly, standard optimal detection assumes prescribed signal shapes s_i , eigenvectors and eigenvalues of the natural variability covariance Σ_v are e_{μ} and λ_{μ} , and the posterior amplitudes α_m and uncertainties Σ_{α} of optimal detection with data vector \mathbf{d} are

$$\begin{aligned}\alpha_m &= \mathbf{G}^{-1}\mathbf{h} \\ \Sigma_{\alpha} &= \mathbf{G}^{-1}\end{aligned}\quad (16)$$

where the elements of matrix \mathbf{G} and vector \mathbf{h} are

$$\begin{aligned}G_{ij} &= \sum_{\mu=1}^k \lambda_{\mu}^{-1} \langle \mathbf{e}_{\mu}, \mathbf{s}_i \rangle \langle \mathbf{e}_{\mu}, \mathbf{s}_j \rangle \\ h_i &= \sum_{\mu=1}^k \lambda_{\mu}^{-1} \langle \mathbf{e}_{\mu}, \mathbf{s}_i \rangle \langle \mathbf{e}_{\mu}, \mathbf{d} \rangle.\end{aligned}\quad (17)$$

Taken together, Eqs. 16 and 17 are the equations of linear multi-pattern regression, or optimal detection. The

α_m is a vector containing scaling factors for each of the signals, the combination of which best explains the data. The angle brackets $\langle \dots, \dots \rangle$ indicate inner products governed by any definition of an inner product as long as the eigenvalues and eigenvectors of Σ , which is defined below, are determined by $\langle \Sigma, \mathbf{e}_{\mu} \rangle = \lambda_{\mu} \mathbf{e}_{\mu}$. The quantity k determines the truncation of the space of detection. With inclusion of signal shape uncertainty, the signal shapes become means of signal shapes as determined by an ensemble of independent climate models, and the uncertainty covariance Σ_u is

$$\Sigma_u = \left\langle \sum_{i,j=1}^m \mathbf{s}_i \mathbf{s}_j^T \right\rangle. \quad (18)$$

(In this case the angle brackets represent averages over an ensemble of signal shapes of independent climate models.) We normalize the signal shapes using an L_1 norm: for each model-predicted signal shape, the sig-

nal is scaled so that its integral over frequency is the same as for the same signal as predicted by all other models. Such a normalization permits a simple interpretation for posterior signal amplitudes α_m : they represent the trends in outgoing longwave radiation associated with the different signals. Accounting for signal shape uncertainty requires that $\Sigma = \Sigma_v + \Sigma_u$ and e_μ and λ_μ are the eigenvectors and eigenvalues of Σ .

In the case of the outgoing longwave spectrum, temperature in the stratosphere and upper tropospheric water vapor are the primary contributors to the signal shape uncertainty Σ_u . The form of temperature change in the stratosphere is substantially different from model to model in the CMIP3 archive because of the variety of implementations of stratospheric ozone. The models' differing schemes of cumulus convection and cloud parameterizations lead to different forms of water vapor trends, especially in the tropical upper troposphere. By accounting for these uncertainties in the signals in the outgoing longwave spectrum, optimal detection essentially searches for other components of the signals for optimization. The final estimate of signals' uncertainties Σ_α will incorporate the signal shape uncertainties as an additional source of "error".

3. Sensitivity analysis

We apply the methodology of optimal detection as described above to the problem of detecting a carbon dioxide signal, a tropospheric warming signal, a stratospheric cooling signal, and a specific humidity signal in outgoing longwave radiance data. The 1801-element data vector is the trend in the annual average outgoing infrared radiance spectrum from 200 to 2000 cm^{-1} with 1 cm^{-1} spectral resolution. Climate models do not simulate the same patterns of change in the infrared spectrum due to trends in the temperature and specific humidity fields, even when spectral trends are normalized by the integral in frequency. Because the tropical troposphere, however, tends to maintain a moist adiabatic temperature profile up to approximately 200 hPa (Xu and Emanuel 1989; Santer et al. 2003), we restrict our analysis to the tropics, which we define to be the global region between 25°S and 25°N, in order to reduce uncertainty in the signal shapes in the infrared spectrum associated with trends in temperature and water vapor.

While it has been conventional to define a lapse rate feedback as distinct from the mean surface air temperature response, in the tropics the two are so strongly correlated that we consider surface air (and surface) temperature response as part of the same signal as the response of tropospheric upper air temperature. With the exception of one of six models, the OLR due to tropical tropospheric temperature trends and tropical sur-

face temperature trends fall onto a straight line with slope $\Lambda = 5.04 \pm 0.06 \text{ W m}^{-2} \text{ K}^{-1}$. This agrees with Held and Soden (2000), who use a global value of $\approx 4 \text{ W m}^{-2} \text{ K}^{-1}$ in their discussion of the water vapor feedback with the negative tropical lapse rate feedback ($\gamma \simeq -1 \text{ W m}^{-2} \text{ K}^{-1}$) considered because $\Lambda = \Gamma - \gamma_{\text{lapse rate}}$, $\gamma_{\text{lapse rate}}$ representing the feedback induced by changes in tropospheric upper air temperature, known as the "lapse rate" feedback. We use this value of Λ in our remaining analysis. One model omitted from the linear fit was omitted because it robustly predicts cooling of the central tropical Pacific sea surface temperature thus biasing its surface temperature trend lower than it would be with a more spatially uniform surface temperature trend.

We apply optimal detection using an estimate of natural variability given by a 400-yr pre-industrial control run of ECHAM5-MPI/OM. In order to reduce the influence of the stratosphere in the optimal detection problem still further, we suppress temperature variations in the stratosphere. We do this by using only the monthly mean value of temperature in the stratosphere, as a function of position, in the radiance calculations. The natural variability covariance was constructed using area-weighted averages over the tropics annually averaged. The first six eigenvectors of the natural variability account for 99.97% of the interannual variability of the outgoing longwave spectrum.

We show the detection amplitudes and uncertainties for the tropospheric temperature and water vapor signals in Fig. 2. The amplitudes α_m and uncertainties Σ_α are scaled by the integral over frequency of the relevant signal used in detection and multiplied by π to account approximately for the integral over solid angle. Conversion of radiance spectra to flux spectra by multiplying by π does not affect our conclusions in any way. The detection assumes a 20-yr continuous timeseries of outgoing longwave spectra, averaged annually over the tropics. The "data" is the timeseries of outgoing longwave spectra simulated using the SRES-A1B output of GFDL CM2.0. Optimal detection is applied using the four signals with mean signal shapes and uncertainty covariance Σ_u determined by six CMIP3 models: GFDL CM2.0, GISS E-H, MIROC 3.2 (medium resolution), ECHAM5-MPI/OM, NCAR CCSM3, and UKMO HadCM3. Fig. 2 shows the effect of increasing the number of eigenvectors of truncation (k in Eq. 17) on signal detection. At least four eigenmodes are required for detection to provide sufficient determinacy. With increasing numbers of eigenmodes retained, the tropospheric temperature radiance trend signal asymptotes quickly to $0.94 \pm 0.42 \text{ W m}^{-2} \text{ decade}^{-1}$ and the water vapor radiance

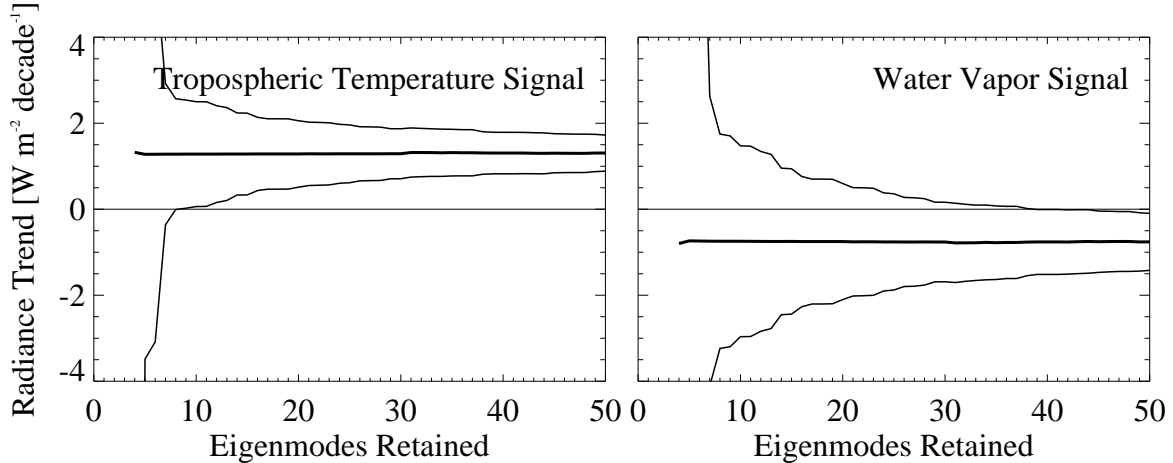


FIG. 2. Optimal detection with signal shape uncertainty taken into consideration. In the plot on the left we show estimates of the tropospheric temperature signal and on the right the water vapor signal as a function of the number of eigenmodes retained in detection. Both amplitudes are scaled by the integral of the signal over frequency and multiplied by π steradians. The thick and thin solid lines show the detection amplitudes with one-sigma uncertainty for signal detection accounting for uncertainty in signal shapes.

trend asymptotes to $-0.59 \pm 0.66 \text{ W m}^{-2} \text{ decade}^{-1}$. The uncertainties are one-sigma uncertainties and account for natural variability. The true numbers for the tropospheric temperature radiance trend and the water vapor radiance trend, found by linear regression of the first 50 years of the SRES-A1B of GFDL CM2.0, are 1.27 and $-0.76 \text{ W m}^{-2} \text{ decade}^{-1}$, respectively.

We show the joint probability of detection of the tropospheric temperature radiance and water vapor signals with 50 eigenmodes retained in detection in Fig. 3. In composing this error covariance ellipse, we have selected the 2×2 sub-matrix of the 4×4 covariance matrix Σ_α (Eq. 16) corresponding to the tropospheric temperature and specific humidity signals. The resulting one-sigma probability ellipse describes the joint probability distribution of detecting these two signals with complete ignorance of the other two signals. A one-sigma ellipse in two-dimensions represents a 39% confidence of detection, the probability that the actual long-term tropospheric temperature and water vapor signals present in the climate of GFDL-CM2.0 fall within this one-sigma ellipse. By including more eigenmodes in detection, we include more information, and the area of the error covariance ellipse must decrease, yet because signal shapes are considered uncertain, the ellipse asymptotes to one with non-zero volume.

The high anti-correlation between the detection of the tropospheric temperature and water vapor signals arises because their signal shapes (c.f. Fig. 1) are similar but opposite in sign. If a positive error is made in esti-

imating the OLR change due to tropospheric temperature change, then the data can only be explained by making an equal and opposite error in estimating the OLR change due to water vapor.

It is more appropriate to estimate posterior uncertainty by detector timeseries analysis than by prescription of natural variability given by a model because detector timeseries analysis is mostly insensitive to a particular prescription of natural variability. In Fig. 4 we show the timeseries of detection amplitudes for each of the four signals as a function of time. We calculate a timeseries of detection amplitudes by computing the inner product of optimal fingerprints with annual average, tropical mean outgoing longwave spectra. The optimal fingerprints are the columns of \mathbf{F} where

$$\begin{aligned} \mathbf{F} &= \mathbf{G}^{-1} \mathbf{H} \\ \mathbf{H}_i &= \sum_{\mu=1}^k \lambda_\mu^{-1} \langle \mathbf{e}_\mu, \mathbf{s}_i \rangle \mathbf{e}_\mu \end{aligned} \quad (19)$$

in which \mathbf{H}_i is the i 'th row of matrix \mathbf{H} . Eq. 19 is to be used in conjunction with Eqs. 16 and 17. The timeseries of detection amplitudes is given by

$$\alpha(t_i) = \langle \mathbf{F}, \mathbf{d}(t_i) \rangle \quad (20)$$

with $\alpha(t_i)$ a timeseries of detectors and the right hand side the inner product of the optimal fingerprints \mathbf{F} on annual average anomaly spectrum $\mathbf{d}(t_i)$. The data anomaly $\mathbf{d}(t_i)$ is just an annual average, tropical average, mean-subtracted outgoing longwave spectrum for

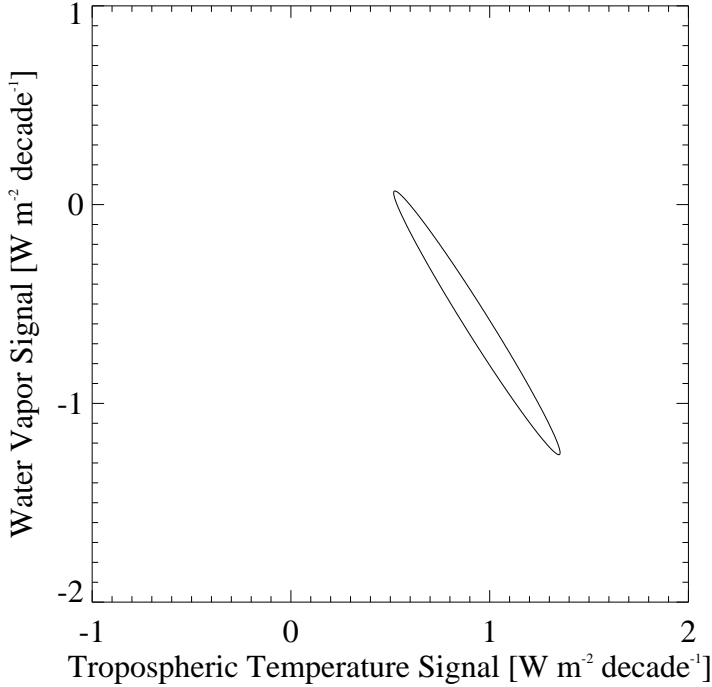


FIG. 3. Detection ellipses for 20-yr trends as simulated by GFDL CM2.0. Detection fingerprints were constructed using the mean signals constructed from the first 50 years of the SRES-A1B forced run of six CMIP3 models and natural variability as constructed from the 400-yr pre-industrial control run of ECHAM5-MPI/OM with stratospheric temperature variability suppressed. Interannual variability is assumed to be mostly uncorrelated from year to year in estimating error covariance ellipses. A $1\text{-}\sigma$ detection ellipse is given for inclusion of 50 eigenmodes in detection. The axes are outgoing longwave radiance trends in time due to tropospheric temperature and water vapor change.

year i . The detection problem is the same as the one posed for Fig. 3. Detection amplitudes are scaled by the integral of the uncertain signals over frequency with an extra factor of π to account approximately for the hemispheric integral. The true outgoing longwave radiation (OLR) anomalies, as determined by PRP directly for the GFDL CM2.0 SRES-A1B run, are also shown for each of the four signals in Fig. 4. The detector timeseries compare favorably to the “truth” timeseries because the signal shapes span a sub-space of the data vector that a large fraction of natural variability occupies. In other words, the typical forms taken by natural fluctuations of the outgoing longwave spectrum look quite similar to the signals we are seeking to detect.

Linear regression of the tropospheric temperature and water vapor signals’ amplitude timeseries enables us to estimate the water vapor-longwave feedback. We find the slopes of the tropospheric temperature amplitude and water vapor amplitude timeseries (α_{temp} and

α_{wv}) in Fig. 4 and then compute the departures of those timeseries ($\delta\alpha'$) from the best fit lines. The uncertainty covariance of the trends α_m is

$$\Sigma'_\alpha = \langle \delta\alpha' \delta\alpha'^T \rangle. \quad (21)$$

The water vapor-longwave feedback is just $\gamma = \Lambda^{-1} \times \alpha_{\text{water vapor}} / \alpha_{T_{\text{trop}}}$, $\alpha_{\text{water vapor}}$ and $\alpha_{T_{\text{trop}}}$ being the elements of α_m multiplying the water vapor and tropospheric temperature signals. The uncertainty in the feedback σ_γ , using the timeseries anomalies as computed in Eq. 21 to estimate error, is

$$\sigma_\gamma^2 = (\nabla_\alpha \gamma)^T \Sigma'_\alpha (\nabla_\alpha \gamma) \quad (22)$$

where $\nabla_\alpha \gamma$ is the Jacobian of γ with respect to α . In the timeseries of detectors shown in Fig. 4, the water vapor longwave feedback is $\gamma = 3.20 \text{ W m}^{-2} \text{ K}^{-1}$ with an uncertainty of $\sigma_\gamma = 1.85 \text{ W m}^{-2} \text{ K}^{-1}$. The “true” water vapor-longwave feedback is $3.30 \pm$

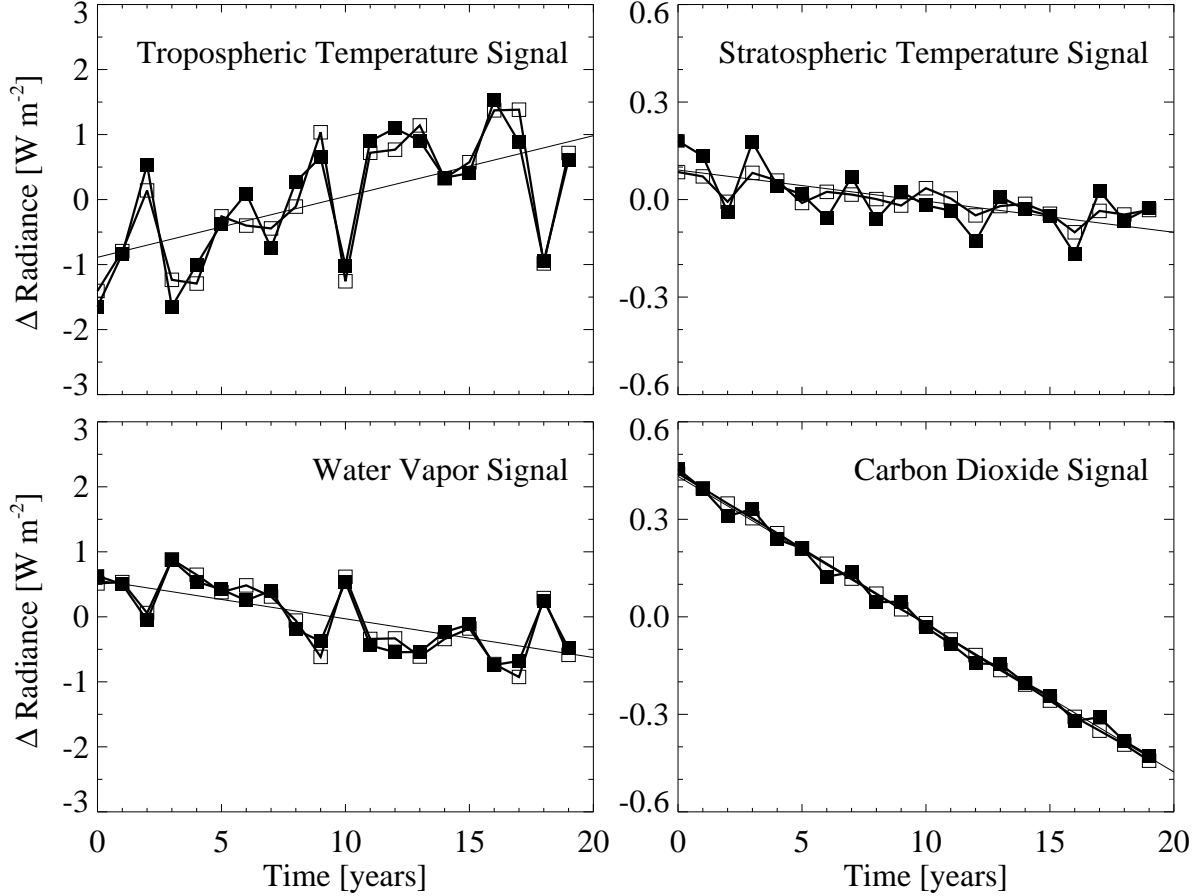


FIG. 4. Detection amplitude timeseries for four signals. The solid squares show detection amplitudes for each of four detected signals. We have converted detection amplitudes to anomalies in outgoing longwave radiation (OLR) by integrating over frequency and multiplying by Λ , which relates fluctuations in surface temperature to fluctuations in outgoing longwave radiation. The open squares show true OLR anomalies for each of the four signals. The thin solid line is the best linear fit to the detection amplitudes and its slopes are in exact agreement with Fig. 3. Note the expanded range for the stratospheric temperature and carbon dioxide signals' amplitudes.

$1.85 \text{ W m}^{-2} \text{ K}^{-1}$ as determined by normal partial radiative perturbation (PRP) analysis on the models' output variables. Even determination of the true water vapor-longwave feedback in a climate model is complicated by the presence of natural variability. As a consequence of the signals spanning much the same space as natural variability, using other models for prescriptions of natural variability and as artificial data does not significantly affect the result that optimal detection of infrared signals takes an inordinately long time to provide a viable test for climate models.

The amplitude timeseries for the tropospheric temperature signal and the water vapor signal are strongly anticorrelated. This is true for both the optimal detection amplitudes (detectors) and the true OLR timeseries, and

so it is a reflection of the physics of the climate system. On time scales of a year, a fluctuation of temperature in the Tropics is directly proportional to radiative forcing by water vapor. In Fig. 5 we show scatterplots of the water vapor detectors vs. tropospheric temperature detectors when using artificial data produced by six CMIP3 models. The artificial data are MODTRAN simulations of the first 20 years of the SRES-A1B runs. Both detectors $\alpha(t_i)$ (see Eq. 20) and true OLR anomalies associated with tropospheric temperature fluctuations and water vapor fluctuations are shown. The strong anticorrelation between the tropospheric temperature signal and the water vapor signal is borne out. The slope of the best fit line divided by Λ , which relates the tropospheric temperature signal to surface air temperature trends, yields

the water vapor-longwave feedback in the tropics, provided that water vapor and temperature are similarly related on yearly and interdecadal timescales. The uncertainty in the determination of the feedback is the uncertainty in the slope of the line in the panels of Fig. 5. The uncertainty is expected to be proportional to the inverse square-root of the number of points in the scatterplot.

In Table 1 we present the results of feedback analysis using simulated data taken from the same six CMIP3 models, comparing the strategies of feedback determination by linear trend analysis and by anomaly correlation analysis. We present “true” evaluations of the feedbacks for context. Both analysis strategies were performed using 20-yr timeseries of simulated data based on SRES-A1B runs of the six models. The uncertainty estimates of the feedback determination by linear trend analysis are due to interannual variability for the “truth” and are primarily due to interannual variability but with a small contribution from errors in optimal detection for the data. On the other hand, the uncertainty estimates of the feedback determination by anomaly correlation analysis are due primarily to small breakdowns in the relationship between tropical temperature and humidity with an additional influence of error caused by signal shape uncertainty. The table demonstrates that a 20-yr trend in outgoing longwave spectra in the tropics will provide a 30% constraint on the water vapor-longwave feedback. Anomaly correlation analysis, though, can provide a constraint of $\approx 5\%$ on the water vapor-longwave feedback in the tropics with a 20-yr timeseries of observations of the outgoing longwave spectrum. Analysis of the water vapor-longwave feedback by anomaly correlation is expected to have accuracy directly proportional to $N^{-1/2}$ where N is the number of years in the timeseries. Thus, with timeseries of infrared spectra in the tropics as short as 10 yrs, it should be possible to distinguish between the climate models of the CMIP3 ensemble whose spread in water vapor-longwave feedback is approximately 20%.

4. Summary and Conclusions

The Earth’s emitted infrared spectrum can be expected to change on interannual time scales in such a way that the relative contribution of various greenhouse gases can be determined. Previous authors have pointed in this direction. We have demonstrated that optimal detection techniques, when applied to trends in the Earth’s emitted infrared spectrum, can yield strong observational constraints on radiative forcing by well-mixed anthropogenic greenhouse gases, carbon dioxide in particular, and the longwave feedbacks of the atmosphere. An optimal detection exercise using simulated data gives estimates of the amount of time necessary be-

fore a timeseries of spectral infrared data is useful for testing climate models.

In our analysis, we have shown that signals associated with radiative forcing by carbon dioxide, tropospheric warming, stratospheric cooling, and the water vapor feedback should be unambiguously discernible in trends in the outgoing longwave spectrum of the tropics. We have used an optimal detection technique that includes an accounting for uncertainty in the longwave spectral signal shapes on artificial data (Huntingford et al. 2006). We are able to distinguish a water vapor radiance signal and the tropospheric temperature radiance signal from the signals due to carbon dioxide forcing and stratospheric temperature response to an accuracy $< 0.1 \text{ W m}^{-2} \text{ ster}^{-1}$. We found that trends in a 20-yr timeseries of annual average, tropical average outgoing longwave spectra will provide a constraint on the water vapor-longwave feedback in the Tropics with $\approx 30\%$ accuracy. The dominant contributor to the accuracy estimate is interannual variability, and the accuracy of the feedback estimate is directly proportional to $(\Delta t)^{-3/2}$, Δt being the length of the timeseries (Leroy et al. 2007). On the other hand, over the same 20 year interval it is possible to establish a relationship between the anomalies in outgoing longwave radiation associated with water vapor and tropospheric temperature, and from that relationship it is possible to estimate a short-term water vapor-longwave feedback to within 5% uncertainty. This latter method’s uncertainty is inversely proportional to the square-root of the length of the timeseries, so a ten-year timeseries can be expected to yield a 7% determination of the tropical water vapor-longwave feedback. The short-term water vapor-longwave feedback agrees with the decadal water vapor-longwave feedback to within error in our study.

Linear trend analysis may give only loose constraints on the water vapor-longwave feedback, but consideration of the spatial component to the longwave spectral signal may provide additional information needed to refine the test. In the case of GPS radio occultation, it was found that poleward migration of the mid-latitude jet streams provided much of the information in detection of climate change (Leroy et al. 2006), and that signal should also be apparent in latitudinal gradients of the tropospheric temperature longwave spectral signal. A spectral-spatial longwave signal analysis should provide more signal-to-noise in detection than just a tropical average spectral longwave signal.

A sound implementation of signal shape uncertainty into optimal detection requires a complete accounting of all sources of uncertainty in climate projection. Models are known to have shortcomings in common, such as an inability to simulate phenomena such as the quasi-

	Linear Trend Analysis ($\text{W m}^{-2} \text{K}^{-1}$)		Anomaly Correlation Analysis ($\text{W m}^{-2} \text{K}^{-1}$)	
	Truth	Data	Truth	Data
	GFDL CM2.0	3.30 ± 1.85	3.20 ± 1.85	2.75 ± 0.20
GISS E-H	2.63 ± 0.81	2.95 ± 0.62	2.61 ± 0.10	2.94 ± 0.12
MIROC 3.2 (medres)	2.81 ± 0.85	2.53 ± 0.62	2.68 ± 0.13	2.49 ± 0.10
ECHAM5-MPI/OM	3.14 ± 1.60	3.53 ± 1.81	2.98 ± 0.08	3.36 ± 0.10
NCAR CCSM3	2.80 ± 0.92	2.81 ± 0.91	2.66 ± 0.17	2.66 ± 0.16
UKMO HadCM3	3.10 ± 1.48	2.65 ± 1.15	2.78 ± 0.09	2.74 ± 0.11

TABLE 1. Water vapor-longwave feedback analysis strategies. We compare linear trend analysis and anomaly correlation analysis as potential strategies for constraining the water vapor-longwave feedback with a timeseries of observations of the outgoing longwave spectrum of the tropics. In linear trend analysis, trends in the tropospheric temperature signal and the water vapor signal are detected in the outgoing longwave spectrum and divided to estimate the water vapor-longwave feedback. In anomaly correlation analysis, a linear relationship is found between interannual anomalies in the detected water vapor signal and interannual anomalies in the detected tropospheric temperature signal. “Truth” is derived from PRP calculations taken directly from climate model output, and “data” is derived from optimal detection in simulated outgoing longwave spectra by MODTRAN based on climate model output.

biennial and Madden-Julian oscillations (Baldwin et al. 2001; Lin et al. 2006), so the climate models contributing to the CMIP3 archive cannot be considered complete in spanning uncertainty in climate prediction. Moreover, we used only six of the CMIP3 models in accounting for signal shape uncertainty, a small number. For this reason, we used one of the same six models to stand in for data to demonstrate the viability of the approach presented herein. In a future application of this methodology to satellite data, it will be necessary to account for a broader space of signal shape uncertainty than is contained in this paper. One possibility is to use the output of a much larger ensemble of climate models such that a more complete spanning of the space of uncertainty is obtained. Another possibility is to expand the space of uncertainty as determined with a small ensemble of climate models artificially by adding variance without additional covariance. In the latter case especially, good judgment is required.

The work presented here is done for clear-sky calculations only, due to limitations of the available archive of CMIP3 model output. The techniques we have used, though, can be expected to work in much the same way for observationally constraining the cloud-longwave feedback, as long as model output is available that is necessary to the simulation of outgoing radiance spectra in cloudy skies. Because the longwave spectral signature of clouds is expected to be very similar to the signature of surface temperature, in realistic cloudy sky conditions it may not be possible to unambiguously determine the temperature response of the climate system in longwave spectra alone. The cloud-insensitive sound-

ing technique of GPS radio occultation may be required as part of the analysis. In any case, we have demonstrated that a timeseries of longwave spectra in as brief a time as ten years should provide a strong constraint on climate models’ realization of longwave feedbacks. If the timeseries of spectral data is intermittent, the detection time is increased depending upon the length of the gaps in the timeseries. If only two annual average snapshots are obtained, Leroy et al. (2007) can be used to show that 13 years between the two snapshots gives the same signal-to-noise of detection as does ten years of continuous data.

Acknowledgments. We acknowledge the modeling groups, the Program for Climate Model Diagnosis and Intercomparison (PCMDI) and the WCRP’s Working Group on Coupled Modelling (WGCM) for their roles in making available the WCRP CMIP3 multi-model dataset. Support of this dataset is provided by the Office of Science, U.S. Department of Energy. This work was supported by grant ATM-0450288 of the National Science Foundation.

References

- Allen, M. and S. Tett, 1999: Checking for model consistency in optimal fingerprinting. *Climate Dyn.*, **15**, 419–434.
- Anderson, J., J. Dykema, R. Goody, H. Hu, and D. Kirk-Davidoff, 2004: Absolute, spectrally-resolved, ther-

- mal radiance: A benchmark for climate monitoring from space. *J. Quant. Spectrosc. Rad. Trans.*, **85**, 367–383.
- Baldwin, M. P., L. J. Gray, T. J. Dunkerton, K. Hamilton, P. H. Haynes, W. J. Randel, J. R. Holton, M. J. Alexander, I. Hirota, T. Horinouchi, D. Jones, J. Kinnerson, C. Marquardt, K. Sato, and M. Takahashi, 2001: The quasi-biennial oscillation. *Rev. Geophys.*, **39**, 179–229.
- Berk, A., L. Bernstein, G. Anderson, P. Acharya, D. Robertson, J. Chetwynd, and S. Adler-Golden, 1998: MODTRAN cloud and multiple scattering upgrades with application to AVIRIS—editions of 1991 and 1992. *Rem. Sens. Env.*, **65**, 367–375.
- Bony, S., R. Colman, V. Kattsov, R. Allan, C. Bretherton, J. Dufresne, A. Hall, S. Hallegatte, M. Holland, W. Ingram, D. Randall, B. Soden, G. Tselioudis, and M. Webb, 2006: How well do we understand and evaluate climate change feedback processes? *J. Climate*, **19**, 3445–3482.
- Charlock, T., 1984: CO₂ induced climatic change and spectral variations in the outgoing terrestrial infrared radiation. *Tellus*, **36B**, 139–148.
- Collins, W., V. Ramaswamy, M. Schwarzkopf, Y. Sun, R. Portmann, Q. Fu, S. Casanova, J. Dufresne, D. Fillmore, P. Forster, V. Galin, L. Gohar, W. Ingram, D. Kratz, M. Lefebvre, J. Li, P. Marquet, V. Oinas, Y. Tsushima, T. Uchiyama, and W. Zhong, 2006: Radiative forcing by well-mixed greenhouse gases: Estimates from climate models in the Intergovernmental Panel on Climate Change (IPCC) Fourth Assessment Report (AR4). *J. Geophys. Res.*, **111**, D14317, doi:10.1029/2005JD006713.
- Colman, R., 2003: A comparison of climate feedbacks in general circulation models. *Climate Dyn.*, **20**, 865–873.
- Dykema, J. and J. Anderson, 2006: A methodology for obtaining on-orbit SI-traceable spectral radiance measurements in the thermal infrared. *Metrologia*, **43**, 287–293.
- Goody, R., J. Anderson, T. Karl, R. Miller, G. North, J. Simpson, G. Stephens, and W. Washington, 2002: Why monitor the climate? *Bull. Amer. Meteor. Soc.*, **83**, 873–878.
- Goody, R., J. Anderson, and G. North, 1998: Testing climate models: An approach. *Bull. Amer. Meteor. Soc.*, **79**, 2541–2549.
- Harries, J., H. Brindley, P. Sagoo, and R. Bantges, 2001: Increases in greenhouse forcing inferred from outgoing longwave radiation spectra of the earth in 1970 and 1997. *Nature*, **410**, 355–357.
- Hasselmann, K., 1993: Optimal fingerprints for the detection of time-dependent climate change. *J. Climate*, **6**, 1957–1971.
- , 1997: Multi-pattern fingerprint method for detection and attribution of climate change. *Climate Dyn.*, **13**, 601–611.
- Hegerl, G., P. Stott, M. Allen, J. Mitchell, S. Tett, and U. Cubasch, 2000: Optimal detection and attribution of climate change: Sensitivity of results to climate model differences. *Climate Dyn.*, **16**, 737–754.
- Held, I. and B. Soden, 2000: Water vapor feedback and global warming. *Ann. Rev. of Energy and Env.*, **25**, 441–475.
- Houghton, J., Y. Ding, D. Griggs, M. Noguer, P. van der Linden, X. Dai, K. Maskell, and C. Johnson, (Eds.) , 2001: *Climate Change 2001: The Scientific Basis, Contribution of Working Group I to the Third Assessment Report of the Intergovernmental Panel on Climate Change*. Cambridge University Press, New York, 881 pp.
- Huntingford, C., P. Stott, M. Allen, and F. Lambert, 2006: Incorporating model uncertainty into attribution of observed temperature change. *Geophys. Res. Lett.*, **33**, doi:10.1029/2005GL024831.
- Kiehl, J., 1983: Satellite detection of effects due to increased atmospheric carbon dioxide. *Science*, **222**, 504–506.
- Kirk-Davidoff, D., R. Goody, and J. Anderson, 2005: Analysis of sampling errors for climate monitoring satellites. *J. Climate*, **18**, 810–822.
- Leroy, S., J. Anderson, and J. Dykema, 2006: Testing climate models using GPS radio occultation: A sensitivity analysis. *J. Geophys. Res.*, **111**, D17105, doi:10.1029/2005JD006145.
- Leroy, S., J. Anderson, and G. Ohring, 2007: Climate signal detection times and constraints on climate benchmark accuracy requirements. *J. Climate*, in press.
- Lin, J., G. Kiladis, B. Mapes, K. Weickmann, K. Sperber, W. Lin, M. Wheeler, S. Schubert, A. Del Genio, L. Donner, S. Emori, J. Gueremy, F. Hourdin, P. Rasch, E. Roeckner, and J. Scinocca, 2006: Tropical intraseasonal variability in 14 IPCC AR4 models. Part I: Convective signals. *J. Climate*, **19**, 2665–2690.

- National Research Council, Committee on Earth Science and Applications from Space, 2007: *Earth Science and Applications from Space: National Imperatives for the Next Decade and Beyond*. National Academies Press, Washington, D.C., 418 pp.
- North, G., R. Cahalan, and J. Coakley, 1981: Energy-balance climate models. *Rev. Geophys.*, **19**, 91–121.
- North, G., K. Kim, S. Shen, and J. Hardin, 1995: Detection of forced climate signals: I. Filter theory. *J. Climate*, **8**, 401–408.
- Pollock, D., T. Murdock, R. Datla, and A. Thompson, 2003: Data uncertainty traced to SI units. Results reported in the International System of Units. *Int. J. Rem. Sensing*, **24**, 225–235.
- Santer, B., T. Wigley, G. Meehl, M. Wehner, C. Mears, M. Schabel, F. Wentz, C. Ammann, J. Arblaster, T. Bettge, W. Washington, K. Taylor, J. Boyle, W. Bruggemann, and C. Doutriaux, 2003: Influence of satellite data uncertainties on the detection of externally forced climate change. *Science*, **300**, 1280–1284.
- Slingo, A. and M. Webb, 1997: The spectral signature of global warming. *Quart. J. Royal Meteor. Soc.*, **123**, 293–307.
- Soden, B. and I. Held, 2006: An assessment of climate feedbacks in coupled ocean-atmosphere models. *J. Climate*, **19**, 3354–3360.
- Stott, P., S. Tett, G. Jones, M. Allen, W. Ingram, and J. Mitchell, 2000a: Anthropogenic and natural causes of twentieth century temperature change. *Space Sci. Rev.*, **94**, 337–344.
- Stott, P., S. Tett, G. Jones, M. Allen, J. Mitchell, and G. Jenkins, 2000b: External control of 20th century temperature by natural and anthropogenic forcings. *Science*, **290**, 2133–2137.
- Tett, S., G. Jones, P. Stott, D. Hill, J. Mitchell, M. Allen, W. Ingram, T. Johns, C. Johnson, A. Jones, D. Roberts, D. Sexton, and M. Woodage, 2002: Estimation of natural and anthropogenic contributions to twentieth century temperature change. *J. Geophys. Res.*, **107**, D164 306, doi:10.1029/2000JD000028.
- Wetherald, R. and S. Manabe, 1988: Cloud feedback processes in a general circulation model. *J. Atmos. Sci.*, **45**, 1397–1415.
- Xu, K. and K. Emanuel, 1989: Is the tropical atmosphere conditionally unstable? *Mon. Wea. Rev.*, **117**, 1471–1479.

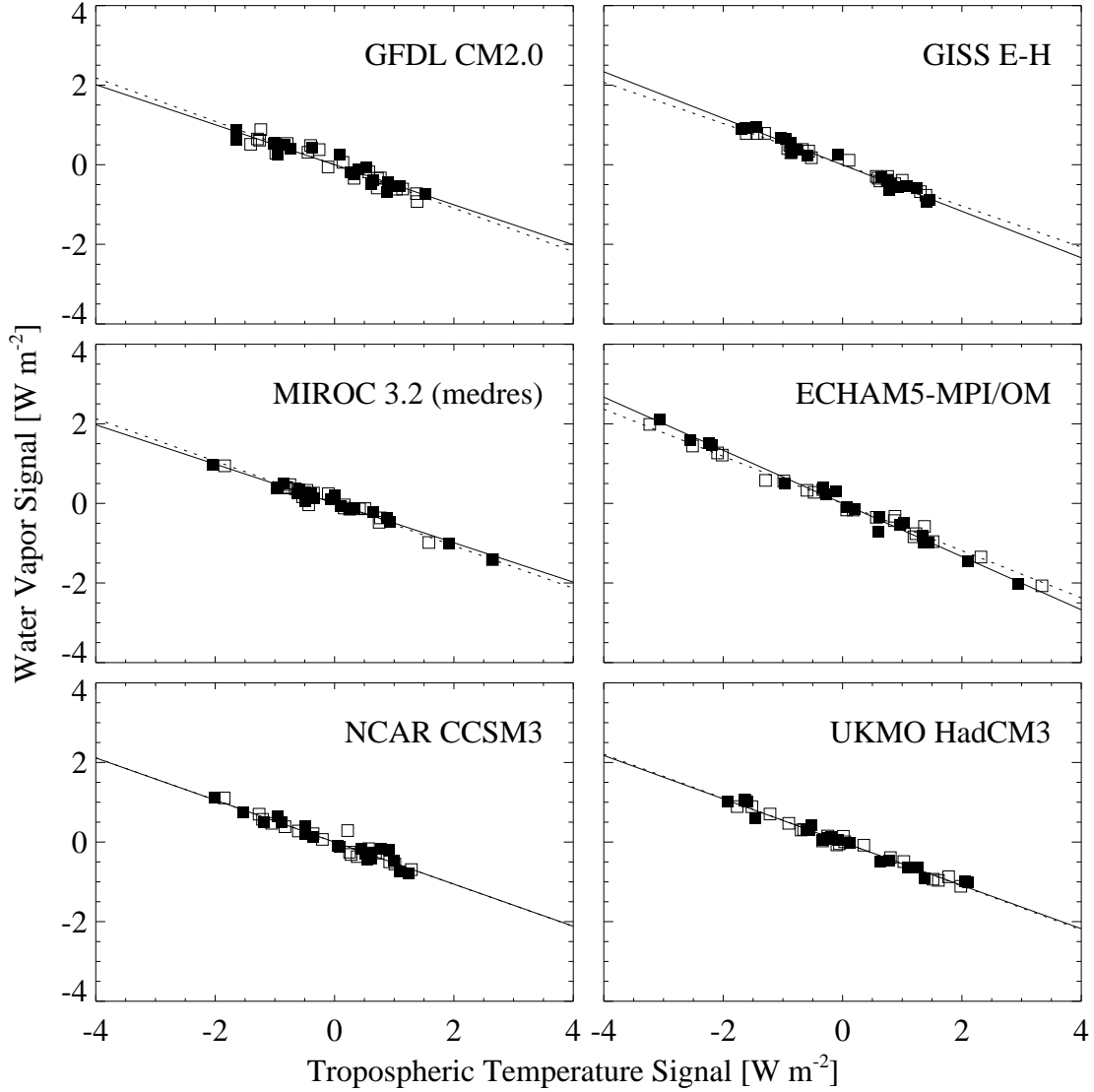


FIG. 5. Water vapor-longwave feedback by anomaly correlation. We have used annual average, tropical average outgoing longwave spectra as simulated by six CMIP3 models as artificial data for optimal detection of OLR contributed by tropospheric temperature and water vapor. For each model, the detection amplitudes are plotted as filled squares and the true OLR anomalies are plotted as open squares. The solid line is the best fit to the detection amplitudes, and the dashed line is the best fit to the true OLR anomalies.